Water Dynamics in a Concentrated Poly(N-isopropylacrylamide) Solution at Variable Pressure

Bart-Jan Niebuur,[†] Wiebke Lohstroh,[‡] Marie-Sousai Appavou,[§] Alfons Schulte,*[,∥][iD] and Christine M. Papadakis*[,†][iD]

[†]Physik-Department, Fachgebiet Physik weicher Materie, Technische Universität München, James-Franck-Str. 1, 85748 Garching, Germany

[‡]Heinz Maier-Leibnitz Zentrum (MLZ), Technische Universität München, Lichtenbergstr. 1, 85748 Garching, Germany

[§]Jülich Centre for Neutron Science (JCNS) at Heinz Maier-Leibnitz Zentrum (MLZ), Forschungszentrum Jülich GmbH, Lichtenbergstr. 1, 85748 Garching, Germany

[∥]Department of Physics and College of Optics and Photonics, University of Central Florida, 4111 Libra Drive, Orlando, Florida 32816-2385, United States

S *Supporting Information*

ABSTRACT: Using quasi-elastic neutron scattering (QENS), we study the dynamics of water in a concentrated poly(N-isopropylacrylamide) solution over a large temperature range across the demixing transition at pressures of 0.1 and 130 MPa. The QENS spectra extending in frequency from 1 to 3×10^3 GHz and in momentum transfer from 0.45 to 1.65 Å^{-1} reveal the relaxation of hydration water as well as multiple dynamic processes in bulk water. At the cloud point, the fraction of hydration water decreases abruptly at 0.1 MPa, whereas at 130 MPa, it decreases smoothly. The susceptibility spectra of hydration water occur at lower frequencies than those of pure water and the dependence of the relaxation times on momentum transfer can be described by a jump-diffusion model. At a pressure of 0.1 MPa, the hydration water remaining in the two-phase region is more constrained than at 130 MPa. We attribute these findings to the pressure-dependent hydration interactions.
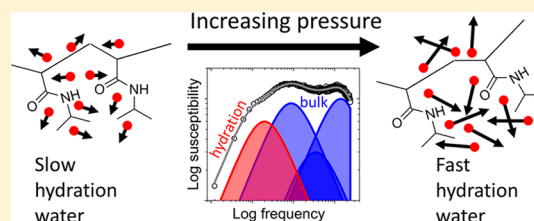
INTRODUCTION

Hydration water is of fundamental importance for the structure and functionality of macromolecules. For instance, it is essential for structural flexibility in the biological action of proteins,[1,2] and it is a key factor for the responsiveness of polymers to external stimuli.[3−5] A comprehensive picture of the water dynamics in the surroundings of macromolecules is therefore paramount for identifying the processes involved in phase transitions of responsive polymers in aqueous solution. The way in which water molecules move may appear as a seemingly general feature of hydration water. Similarly to pure water,[6−9] hydration water molecules may diffuse through jumps between cages formed by neighboring molecules. Between these jumps, the water molecules stay in place and perform a local motion.[10−12]

The motion of water molecules in the hydration shell of macromolecules is, however, constrained with respect to bulk water; i.e., their motion is spatially and/or temporally hindered.[10,12] The diffusive properties of hydration water depend strongly on the type of macromolecule under consideration: In the case of proteins in their native state, the presence of a shell with a certain roughness and disorder leads to anomalous subdiffusion of hydration water; i.e., the mean-square displacement is nonlinear in time.[1,13−15] In polymer solutions[16−18] or solutions of small molecules,[19]

where such surface structures are much less pronounced, a broad distribution of normal diffusive processes is often observed instead. These two cases show that the structure of the solute influences the hydration water strongly.

The dynamics of hydration water at phase transitions in polymer solutions have only sparsely been investigated. Here, we address the phase behavior of the thermoresponsive polymer poly(N-isopropylacrylamide) (PNIPAM) in aqueous solution around its cloud point. At atmospheric pressure, PNIPAM shows lower critical solution temperature (LCST) behavior with a critical temperature of ∼32 °C.[20] The solubility of PNIPAM is governed by the competing, temperature-dependent hydration of hydrophilic and hydrophobic groups.[20,21] In the one-phase region, PNIPAM exhibits a coil-like conformation due to the hydration of both hydrophilic and hydrophobic groups. When the two-phase region is reached by heating through the cloud point, cooperative dehydration of hydrophobic groups causes the chains to collapse, which is followed by the aggregation of the chains.[22,23] The hydrophilic groups retain a substantial amount of hydration.[21,23,24] Changes of the dynamic properties of

water at the phase transition were probed using quasi-elastic neutron scattering (QENS)[11,25] and dielectric relaxation spectroscopy (DRS).[26] At the phase transition temperature, the fraction of hydration water was found to steeply decrease; i.e., the chains dehydrate. The mobility of the remaining hydration water is strongly reduced with respect to bulk water.[11,26−28]

The hydration properties of PNIPAM in aqueous solution also depend on pressure. The coexistence line in the pressure−temperature plane is an ellipse with a maximum at ∼65 MPa and ∼35 °C.[29−33] At pressures beyond the maximum, other mechanisms than the mentioned ones may become dominant in the phase separation of aqueous PNIPAM solutions. Because of the weakening of the hydrophobic effect at high pressure,[34−38] the chains stay hydrated in the phase-separated state.[39,40] This results in the formation of larger aggregates that contain more water than at atmospheric pressure.[40] At high pressure, the driving force behind phase separation may therefore include other factors than dehydration, and thus the hydration water plays a different role than at atmospheric pressure. MD simulations suggested that the driving force for pressure-induced phase separation is the reduction of excess volume of PNIPAM chains in water upon aggregation.[41]

Both temporal and spatial variables determine the dynamic structure of hydration water. Quasi-elastic neutron scattering (QENS) is thus a method of choice to investigate its dynamics, since it covers the relevant time and length scales. Previous QENS investigations of aqueous PNIPAM solutions at temperatures around the cloud point in dependence on pressure[25] were limited by narrow ranges in both energy and momentum transfer. It was found, though, that high pressure leads to a gradual phase transition due to the weakening of hydrogen bonding of water molecules. In this study, we employ QENS over an extended range of momentum and energy transfer to investigate the role of hydration water in a concentrated aqueous PNIPAM solution through temperature scans around the cloud point at both atmospheric and high pressure of 130 MPa, i.e., on the left and on the right side of the maximum of the elliptical coexistence line.

Characterization of the hydration water is complicated by the presence of bulk water dynamics that already comprises three processes.[42] We therefore selected an energy window of our QENS experiment that spans more than 3 decades and convert the dynamic structure factors into the dynamic susceptibilities. This representation allows a more transparent separation of polymer−water contributions from those of bulk water in dependence on temperature and pressure.

The paper is organized as follows: After the Experimental Section, the overall features of the QENS experiments as well as the procedures for data analysis are discussed. In the first part of the Results section, we analyze the dynamics of pure water at ambient and high pressure. The main part of the Results section deals with the water dynamics in the PNIPAM solution. Here, the relative fraction of hydration water and its relaxation time in dependence on temperature and pressure are evaluated. Finally, the chain dynamics are discussed. Conclusions on the behavior of the hydration water around the demixing transition in dependence on pressure are presented at the end.

EXPERIMENTAL SECTION

Materials. Poly(N-isopropylacrylamide) with a molar mass M_n = 36 kg mol^{-1} and a dispersity of 1.26 (end groups carboxylic acid and a

hydrogen atom, respectively) was purchased from Sigma-Aldrich. The polymer was dissolved in deionized H$_2$O at a polymer concentration of 25 wt %. At this concentration, the molar ratio of NIPAM monomers to water molecules equals 1:19. From the calculated values of the coherent and incoherent scattering cross sections (listed in Table 1), it follows that 77% of the detected neutrons were scattered by H$_2$O. Because of the large incoherent cross section of hydrogen, the coherent contribution to the spectra can be neglected. For comparison, pure H$_2$O was measured under the same conditions.

Table 1. Calculated Coherent and Incoherent Neutron Scattering Cross Sections for NIPAM Monomers and Water[a]

| compound	composition	incoherent cross section σ_i [b]	coherent cross section σ_c [b]
NIPAM	C$_6$H$_{11}$NO	883.54	67.89
water	H$_2$O	160.54	7.74

[a]Calculations are based on the scattering cross sections in ref 43.

Quasi-Elastic Neutron Scattering (QENS). QENS measurements were conducted at the time-of-flight spectrometer TOFTOF at the FRM II, Garching, Germany.[44,45] A wavelength of the incident neutron beam of 6 Å along with a rotation speed of the chopper system of 14000 rpm was selected. With these configurations, an elastic energy resolution of ∼0.03 meV (HWHM) and energy transfers from −10 to 1.5 meV were obtained; i.e., the measurements were performed at the system energy-loss side.

The sample was mounted in an aluminum (EN AW-7075) pressure cell, suitable for pressures up to 200 MPa,[46] and was placed at an angle of 135° with respect to the incident neutron beam. Heating scans from ∼27 to ∼55 °C were performed in steps of 1−3 °C at atmospheric pressure (0.1 MPa) and at 130 MPa. The cloud points are at T_{cp} = 31.4 ± 0.1 and 34.1 ± 0.1 °C for 0.1 and 130 MPa, respectively, as determined by turbidimetry (for details, see the Supporting Information). The measuring time at each temperature was 60 min at atmospheric pressure and 120 min at 130 MPa with 30 min equilibration time after each temperature change. Pure H$_2$O was measured as a reference at selected temperatures at both pressures. The signal was recorded with ∼1000 He^3 detector tubes, covering an angle from 7.5° to 140°. The shadow area of the cell around 135° was excluded, which resulted in an accessible range of momentum transfers, q, from 0.15 to 1.65 Å^{-1}. The spectra were normalized to the incoming neutron flux and a vanadium standard measurement. An empty pressure cell measurement was performed and was subtracted from the data. The time-of-flight data recorded by the detectors were then converted to energy transfers of the neutrons, normalized to the energy-dependent detector efficiency and binned in groups of equal Δq. The empty pressure cell and a thin vanadium slab were measured to perform background corrections and calibrations. These operations were performed using the TOFTOF data reduction routines within Mantid.[47]

RESULTS AND DISCUSSION

Overall Features of QENS Spectra. The dynamics of water in a 25 wt % PNIPAM solution in H$_2$O is investigated with quasi-elastic neutron scattering (QENS) at atmospheric pressure (0.1 MPa) and at 130 MPa around the respective cloud point temperatures. The polymer concentration of 25 wt % corresponds to a molar ratio of NIPAM monomers to water molecules of 1:19. In several experiments, though, the number of water molecules that on average interact with each PNIPAM monomer was found to be 11 in the one-phase region.[23,26,28,48,49] Therefore, a significant part of water in a 25 wt % PNIPAM solution is expected to be hydration water. To assign the measured quasi-elastic signal in the polymer solution to the different species of water, the spectra of pure
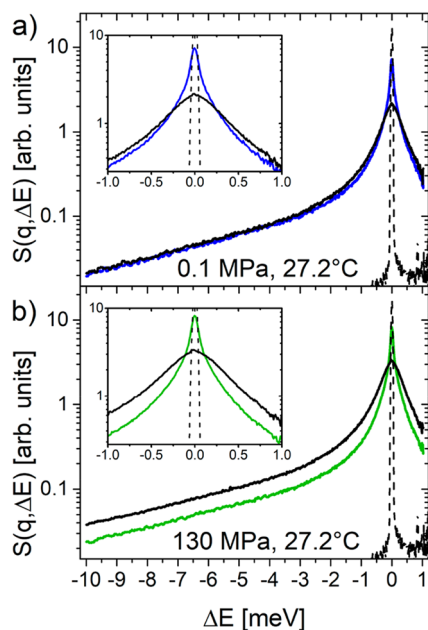
Figure 1. Dynamic structure factor $S(q,\Delta E)$ of H_2O (black full line) and the 25 wt % PNIPAM solution in H_2O at $q = 1.65$ Å^{-1} and 27.2 °C at 0.1 MPa (a, blue line) and 130 MPa (b, green line). The insets show $S(q,\Delta E)$ in a narrower range of ΔE. Black dashed line: elastic line from the measurement on vanadium.

water at the same temperatures and pressures are used as a reference. Figure 1 depicts the dynamic structure factors $S(q,\Delta E)$ at $q = 1.65$ Å^{-1} of pure water and of the 25 wt % PNIPAM solution at 27.2 °C at 0.1 MPa (Figure 1a) and 130 MPa (Figure 1b), i.e., in the one-phase region. At both pressures, clear differences between pure water and the 25 wt % PNIPAM solution are evident: The dynamic structure factor of the 25 wt % PNIPAM solutions shows an enhanced intensity at low energy transfers (below 0.25 and 0.12 meV for 0.1 and 130 MPa, respectively), indicating the presence of slowly moving moieties. These are tentatively attributed to both hydration water and the polymer segments. Thus, the dynamic structure factor of aqueous PNIPAM solutions is composed of several contributions that in a simple approximation could be modeled by a superposition of Lorentzian line shapes.[11,25,50]

The different processes can be distinguished better when the dynamic structure factor is transformed into the imaginary part of the corresponding dynamic susceptibility, $\chi''(q,\nu)$. This has become common practice for liquids and aqueous solutions of biomacromolecules,[13,19,51−54] and it also allows for direct comparison with spectroscopic data. The frequency ν follows from the energy shift as $\nu = \Delta E/h$ where h is Planck's constant. Taking into account the detailed-balance factor, $\chi''(q,\nu)$ is related to $S(q,\nu)$ on the system energy-loss side by the fluctuation−dissipation theorem via the relation[42]

$$\chi''(q, \nu) \propto \frac{S(q, -\nu)}{n_B(\nu)} \tag{1}$$

where n_B is the Bose factor,[55]

$$n_B = \left[\exp\left(\frac{h\nu}{k_B T}\right) - 1\right]^{-1} \tag{2}$$

with k_B being Boltzmann's constant and T the absolute temperature. In this representation, the weighting with the Bose factor reduces the elastic contribution,[56] and the dynamic processes of water are more easily discernible. Accordingly, the data are presented and analyzed in the form of susceptibility spectra.

QENS Spectra of Pure Water. For a clear separation of the bulk and the hydration water in the dynamic properties of PNIPAM solutions, we carefully conducted QENS measurements of pure H_2O at atmospheric and high pressure in the same sample cell as the PNIPAM solution and analyzed the data in the same way. Figure 2 shows the susceptibility spectra at $q = 1.65$ Å^{-1} of pure H_2O measured at 0.1 (a) and 130 MPa (b) at both 27.2 and 55.2 °C, i.e., below and above the cloud point of the PNIPAM solution.
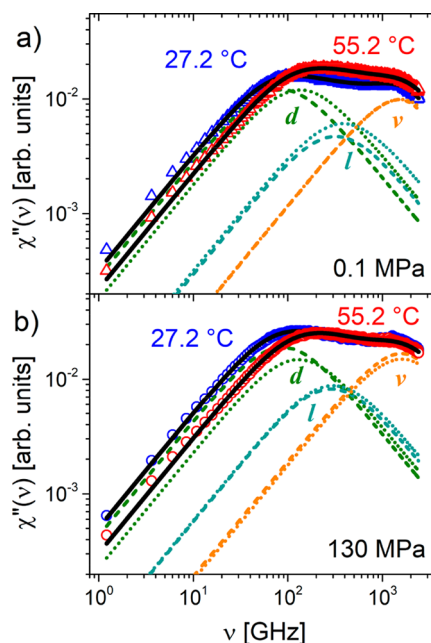
Figure 2. Dynamic susceptibilities of pure H_2O measured at $q = 1.65$ Å^{-1} at 0.1 MPa (a) and 130 MPa (b). For each pressure, data at two temperatures are displayed: at 27.2 °C (blue symbols) and at 55.2 °C (red symbols). Full black lines: cumulative fits of eq 3. Deconvoluted contributions to the fitting function: diffusive process d (olive lines), effective local process l (turquoise lines), and a vibrational process v (orange lines) with dashed lines for 27.2 °C and dotted lines for 55.2 °C.

In pure H_2O, three relaxation processes can be distinguished over the frequency range from 1 to ∼5000 GHz: a diffusional process (marked d in Figure 2) centered at ∼8 × 10^1 GHz, an effective local process (l) centered at ∼3 × 10^2 GHz, and a vibrational process (v) centered at ∼2 × 10^3 GHz, in accordance with ref 42. Therefore, the susceptibility spectra of pure H_2O are modeled by the following function:

$$\chi_q''(\nu) = \chi_{q,d}''(\nu) + \chi_{q,l}''(\nu) + \chi_{q,v}''(\nu) \tag{3}$$

Both the diffusional process and the effective local process are parametrized by Debye functions:

$$\chi_{q,i}''(\nu) = -\text{Im}\left\{C_{q,i}\frac{1}{1 + 2\pi i\tau_i\,\nu}\right\} \tag{4}$$

where $C_{q,i}$ is a q-dependent scaling factor. τ_i denotes the relaxation time, which is related to the peak frequency by $\tau_i = (2\pi\nu_{max})^{-1}$. The index i stands for d or l. The Debye function describes a homogeneous relaxation process, i.e., a single-exponential decay in the time domain.[57] A damped harmonic oscillator (DHO) function accounts for the vibrational relaxation process:[54,58]

$$\chi''_{q,v}(\nu) = -\text{Im}\left\{ C_{q,v} \nu_0^2 \frac{1}{\nu^2 - \nu_0^2 - (i\nu\Gamma/2\pi)} \right\} \quad (5)$$

with $C_{q,v}$ a scaling factor, ν_0 the peak frequency, and Γ the width at half-maximum. The vibrational process was previously assigned to intermolecular O−O−O bending vibrations[59−61] and therefore reflects the stiffness of the hydrogen bonding network.[62]

The fits of eq 3 to the susceptibility spectra of pure H_2O are shown in comparison with the data in Figure 2. The effective local process and the vibrational process change position only slightly with temperature, whereas a clear dependence on temperature is observed for the diffusive process at both 0.1 and 130 MPa: At 55.2 °C, the peak is shifted to higher frequencies, meaning that the diffusion becomes faster with increasing temperature, as expected. The q dependences of the relaxation times of the diffusive and the effective local process are displayed in Figure 3a.

For both temperatures, the relaxation time $\tau_d(q)$ approaches a q^{-2} behavior at low q values, confirming that the peak at low frequencies indeed has the characteristics of a diffusive relaxation process. At higher q values, the dependence becomes weaker, pointing to a more localized process at high q values.
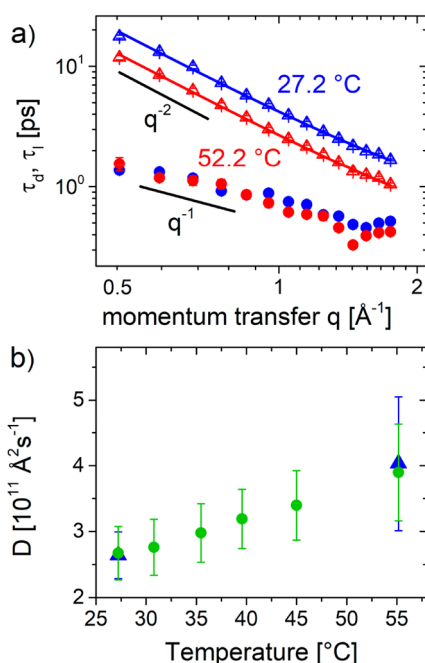
Figure 3. Results on pure H_2O. (a) Relaxation times of the diffusive process (triangles) and of the effective local process (circles) in dependence on the momentum transfer q at 0.1 MPa at 27.2 °C (blue symbols) and at 55.2 °C (red symbols). Full lines: fits of the isotropic jump model (eq 6) to the data of the diffusive process. (b) Diffusion coefficients from the isotropic jump model at atmospheric pressure (blue triangles) and 130 MPa (green circles).

This behavior, where water molecules perform local motions for a certain time before they rapidly jump to a new position, can be described by the isotropic jump model:[6,9,63]

$$\tau = \tau_0\left[1 + \frac{6}{q^2 l^2}\right] \quad (6)$$

where the residence time τ_0 and an apparent jump length l relate to both the translational displacement and the residence time distribution. In the low q limit, a purely diffusive process is observed with diffusion coefficient $D = l^2/(6\tau_0)$. Although this model is strongly simplified, e.g., concerning the mechanism of the jumps,[9] and its validity has been under debate,[8,64] it has been successfully used to describe the diffusion of bulk water molecules in wide ranges of temperature[7,9] and pressure.[65,66] The jump diffusion model is useful for quantitative comparison because it can also be applied to the diffusion of hydration water of PNIPAM, as will be discussed below.

The residence time and apparent jump length of pure water, $\tau_{0,d}$ and l_d, are obtained from the fits with eq 6. The fits are exemplarily shown in Figure 3a, while $\tau_{0,d}$ and l_d are displayed in Figures 8a and 8b. At both pressures, $\tau_{0,d}$ decreases from ∼0.4 to ∼0.2 ps with increasing temperature, whereas l_d scatters around an average value of 0.75 Å. The diffusion coefficients are given in Figure 3b. The values obtained at 0.1 MPa, namely $D = (2.6 \pm 0.4) \times 10^{11}$ Å^2 s^{-1} at 27.2 °C and $D = (4.0 \pm 1.1) \times 10^{11}$ Å^2 s^{-1} at 55.2 °C, are in excellent agreement with literature values.[67−69] The diffusion coefficients measured at 0.1 and 130 MPa are equal within the uncertainties, in accordance with literature data.[70] The relaxation time of the effective local process depends only weakly on q, namely approximately like q^{-1} (Figure 3a). Several theories were put forward to explain the physical nature of this process,[71−74] but no consensus has been reached yet.

These results are in agreement with other studies on the dynamic behavior of water and validate the procedure used for the analysis of the QENS data. We now proceed to the analysis of water dynamics in the PNIPAM solution.

Dynamic Properties of Water in a PNIPAM Solution. The 25 wt % PNIPAM solution in H_2O was measured under the same experimental conditions as the pure H_2O sample. The dynamic properties of water in the solution are expected to change considerably, since a large fraction of the water molecules are close to the polymer, and polymer−water interactions become significant. Figure 4a shows the dynamic structure factors $S(q,\Delta E)$ at a q value of 1.65 Å^{-1} in dependence on temperature at 0.1 MPa. These are transformed into susceptibility spectra according to eq 1 and are shown in Figure 4b. In the latter, a strong relaxation peak at low frequencies is observed at low temperatures (27−36 °C), indicating the presence of a large fraction of hydration water. At 37 °C, this contribution decreases sharply in intensity, suggesting that the chains dehydrate strongly. We attribute this change to the phase transition at the cloud point temperature, which is measured as $T_{cp} = 31.4 \pm 0.1$ °C by turbidimetry. (We cannot exclude a small discrepancy in the temperature calibration of the pressure cell used for QENS measurements and the one used for turbidimetry, since the geometry of the QENS pressure cell allows neither proper insulation nor a temperature measurement at the sample position.) At the phase transition, hydrogen bonds between PNIPAM and water are broken and, instead, inter- and intrachain bonds are
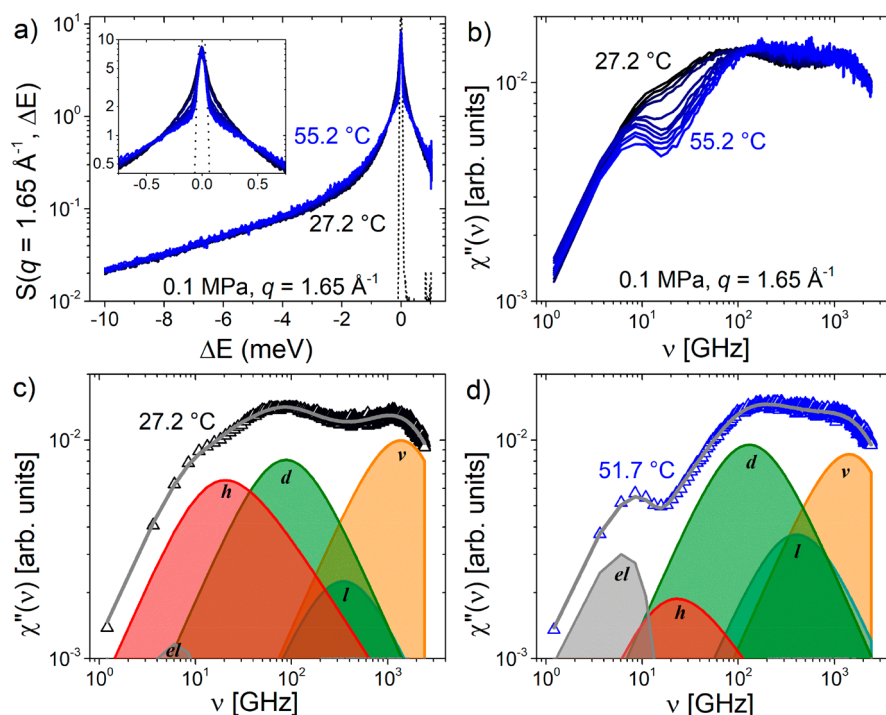
Figure 4. (a) Dynamic structure factors $S(q,\Delta E)$ of the 25 wt % PNIPAM solution in H_2O at $q = 1.65$ Å^{-1} and 0.1 MPa in dependence on temperature during a heating scan. From black to blue: 27.2, 30.0, 32.4, 35.5, 37.4, 39.6, 42.3, 45.0, 48.4, 51.7, and 55.2 °C. The inset shows $S(q,\Delta E)$ at the same temperatures in the region close to the elastic line. Black dashed line: elastic line from the measurement on vanadium. (b) Susceptibility spectra determined from (a) according to eq 1. Example fits according to eq 7 (dark gray line) and the deconvolutions of the fits into their individual components at 27.2 °C (c) and 51.7 °C (d). Elastic fraction el (gray), hydration water relaxation h (red), diffusive process of pure water d (olive), effective local process of pure water l (turquoise), and a vibrational process v (orange).

formed, leading to dehydration and consequently aggregation of the polymers.[24,75,76] Cooperative effects, mediated by the backbone, were found to play a role.[22,23,77] At high temperatures, however, a weak contribution at low frequencies remains, which is attributed to scattering from very slowly moving moieties.

Thus, in comparison to pure water, two additional processes are discernible in the low-frequency range (below ~50 GHz) at low temperatures: (I) Relaxation processes significantly slower than the ones of bulk water are observed in the frequency region ~10−100 GHz. These can be attributed to hydration water, i.e., water that has bonding interaction with the polymeric chains. (II) At very low frequencies, scattering from very slowly moving moieties is visible, which may be attributed to scattering from the polymers, but may also contain contributions from strongly bound water. Previous QENS experiments with high energy resolution on PNIPAM microgels uncovered dynamic processes of the chains with diffusion coefficients that correspond to contributions in the susceptibility representation at ~0.2 and ~1.8 GHz at $q = 1.65$ Å^{-1}.[78] Although these frequencies cannot be resolved in our experiment, it cannot be excluded, that fast dynamic processes of PNIPAM in the one-phase state give a weak contribution to the quasi-elastic signal.

For the analysis of the measured dynamic susceptibility spectra, the instrumental resolution has to be considered. To take this into account, especially for the hydration water dynamics (I), a reasonable approximation is to use only points above ν_{res}, defined as the HWHM of the resolution function.[19] In the present case, $\nu_{res} = 7$ GHz, which is much smaller than the peak frequency of ~20 GHz of the relaxation process of

hydration water. Because the very slow processes (II) are beyond the resolution limit of the experiment, they appear within the elastic scattering whose line shape is given by the measured resolution function. The elastic line is indistinguishable from the resolution function measured with a vanadium standard. Therefore, we chose to include the measured resolution function in the deconvolution of the dynamic susceptibility and vary its amplitude in fits of the PNIPAM solution, in a similar way as in a previous study.[53]

Thus, the susceptibility spectra of the PNIPAM solution were modeled with the expression

$$\chi_q''(\nu) = \chi_{q,el}''(\nu) + \chi_{q,h}''(\nu) + \chi_{q,d}''(\nu) + \chi_{q,l}''(\nu) + \chi_{q,v}''(\nu)$$

(7)

where the diffusional and the local processes of the bulk water fraction $\chi_{q,d}''(\nu)$ and $\chi_{q,l}''(\nu)$ were described by Debye functions (eq 4) and the vibrational process of the bulk water fraction $\chi_{q,v}''(\nu)$ by a DHO function (eq 5). $\chi_{q,el}''(\nu)$ is the measured resolution function multiplied by a constant $C_{q,el}$:

$$\chi_{q,el}''(\nu) = C_{q,el}\, \chi_{q,Res}''(\nu)$$

(8)

The contribution from the relaxation of the hydration water, $\chi_{q,h}''(\nu)$, may be described by a Debye function (eq 4), thereby assuming dynamic homogeneity of the hydration water. However, in dielectric studies of aqueous solutions of PNIPAM in the one-phase region[26] and of other water-soluble macromolecules,[2] it was observed that the hydration water exhibits dynamic heterogeneity, i.e., a distribution of relaxation times. The relaxation of hydration water is well described by a Cole−Davidson function, which reads
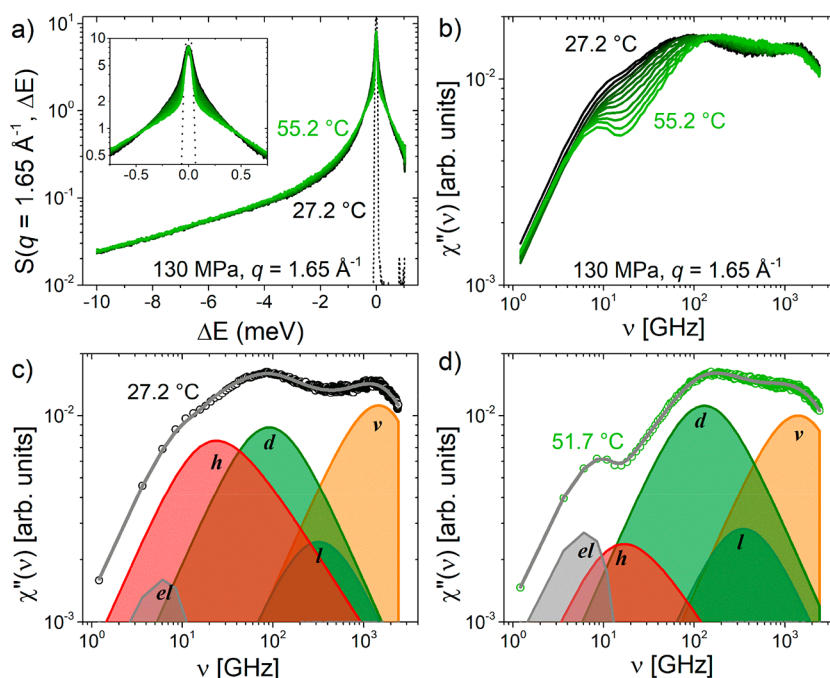
Figure 5. (a) Dynamic structure factors $S(q,\Delta E)$ of the 25 wt % PNIPAM solution in H_2O at $q = 1.65$ Å^{-1} and 130 MPa in dependence on temperature during a heating scan. From black to blue: 27.2, 30.0, 32.4, 35.5, 37.4, 39.6, 42.3, 45.0, 48.4, 51.7, and 55.2 °C. The inset shows $S(q,\Delta E)$ at the same temperatures in the region close to the elastic line. Black dashed line: elastic line from the measurement on vanadium. (b) Susceptibility spectra determined from (a) according to eq 1. Example fits according to eq 7 (dark gray line) and the deconvolutions of the fits into their individual components at 27.2 °C (c) and 51.7 °C (d). Same notation as in Figure 4.

$$\chi''_{q,h}(\nu) = -\mathrm{Im}\left\{ C_{q,h}\frac{1}{(1 + 2\pi i\tau_h\,\nu)^\alpha} \right\} \tag{9}$$

with $C_{q,h}$ a scaling constant, τ_h the relaxation time, and α the stretching exponent. In the susceptibility spectrum, this dynamic heterogeneity appears as broadening of the peak at the high-frequency side. Preliminary fits with the contribution of the hydration water modeled by a Debye function or a Cole−Davidson function (Figure 4) showed that the latter describes the susceptibility of the hydration water best when the exponent takes values of $\alpha = 0.65-0.75$, resulting in an excellent fit over the entire range. Thus, for the analysis of all spectra, we used a value of $\alpha = 0.7$ (see the Supporting Information for a more detailed discussion).

During the fits, the relaxation times of the diffusive and effective local process of bulk water were kept constant, using interpolated values from the measurements of pure water for the actual temperature. Furthermore, the fraction of hydration water as well as the peak frequency ν_0 and the peak width Γ of the DHO term were assumed to be independent of q. Because the different contributions were clearly separated at high q values, we fitted the spectra at $q = 1.45$, 1.55, and 1.65 Å^{-1} first and used the mean values from these fits for the entire q range.

Fits of eq 7 reveal details about the contributions of the individual components (for more q values, see the Supporting Information). At 27.2 °C (Figure 4c), the spectrum is dominated by the contribution from hydration water. The deconvolutions are shown exemplarily for the measurements at $q = 1.65$ Å^{-1} in the one-phase region at 27.2 °C (Figure 4c) and deep in the two-phase region at 51.7 °C (Figure 4d). The measurement at 51.7 °C (Figure 4d) confirms that the amount of the hydration water is decreased. Scattering from these water molecules may contribute both to the elastic line and to

the signal of the bulk water: The increase of the elastic fraction (as inferred from the fit of its amplitude) is presumably due to water molecules trapped inside the polymer-rich domains that are formed in the two-phase region and are strongly restricted in their motion. The release of hydration water into bulk water is evident from the increase of the amplitude of the bulk water peak with relaxation times $\sim 10^2-10^3$ GHz.

Figures 5a and 5b show the dynamic structure factors and susceptibility spectra obtained at $q = 1.65$ Å^{-1} and 130 MPa in dependence on temperature. At low temperatures, the presence of hydration water is evident from the enhancement of the susceptibility at low frequencies (below ∼50 GHz), which changes its character at high temperatures. Contrary to the measurement at 0.1 MPa, the transition at the cloud point is not sharp but rather gradual. The same fitting procedure is used as for 0.1 MPa, with results shown exemplarily for 27.2 and 51.7 °C in Figures 5c and 5d at $q = 1.65$ Å^{-1} (for more q values, see the Supporting Information). The overall dynamic properties do not differ significantly from the measurements at the same temperatures at 0.1 MPa in that the same relaxations are observed.

Relative Populations of Hydration and Bulk Water. Because the amplitudes C_i of the different contributions to the total susceptibility are proportional to the respective scattering intensities, the relative populations of the different types of hydration and bulk water, f_i, are determined as

$$f_i = \frac{C_{q,i}}{C_{q,h} + C_{q,d} + C_{q,l}} \tag{10}$$

with $i = h$, d, or l using the averaged values obtained from the measurements at $q = 1.45$, 1.55, and 1.65 Å^{-1}. At both pressures, the intensities of the vibrational process in the 25 wt % PNIPAM solution are similar to the one of pure water; see

for instance the deconvolutions of the spectra below and above T_{cp} (Figures 2, 4c,d, and 5c,d). Both bulk water and hydration water may contribute to the vibrational process that is therefore not included in the calculation of the relative populations. The elastic fraction is not considered either. We note that since the amount of trapped water in the two-phase region is significant, as follows from the increase of the elastic line strength at T_{cp}, the amount of water molecules considered for the determination of the relative fractions of hydration and bulk water is not constant over the entire temperature range. The values of the relative populations should therefore be taken with caution. Figure 6a shows the resulting relative
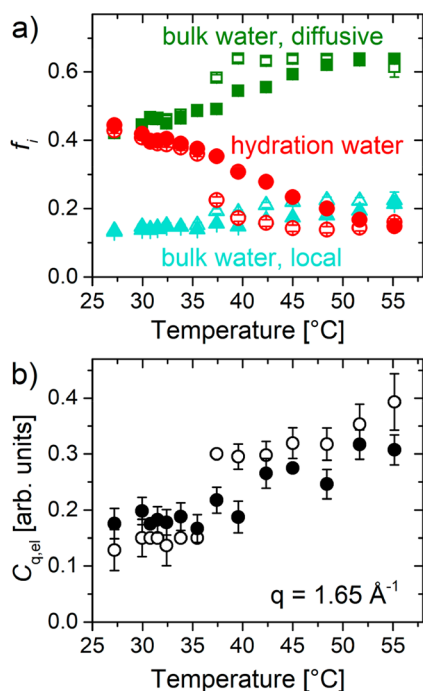
Figure 6. (a) Relative populations f_i of different water species, averaged over the measurements at $q = 1.45$, 1.55, and 1.65 Å^{-1}, determined according to eq 10 in dependence on temperature. Red circles: hydration water; olive squares: diffusive contribution to bulk water; and turquoise triangles: effective local contribution to bulk water. Open symbols: 0.1 MPa; closed symbols: 130 MPa. (b) Elastic line strength in dependence on temperature for 0.1 MPa (open symbols) and 130 MPa (closed symbols) at $q = 1.65$ Å^{-1}.

populations of hydration water, of the diffusive process of bulk water, and of the effective local process of bulk water in dependence on temperature for the two pressures investigated.

At atmospheric pressure (open symbols in Figure 6a), the relative population of the hydration water far below T_{cp} (e.g., at 27.2 °C) is ~0.45 with a weak trend toward lower values with increasing temperature, which is similar to the ratio of bound water molecules obtained with other methods (~11 per PNIPAM monomer[23,26,28,48,49]) and the overall amount of 19 water molecules per monomer in the sample. At 37 °C, the ratio decreases sharply to ~0.2, as expected for PNIPAM solutions at atmospheric pressure.[11,22] However, this decrease occurs ~4 K above the cloud point temperature determined from turbidimetry ($T_{cp} = 31.4$ °C). In spite of careful calibration, there may be a small mismatch in temperature calibration between the pressure cells used for turbidimetry and QENS. Still, as mentioned above, these results suggest that

the dehydration of the chains occurs when aggregates have already formed. Similar results were found by Raman spectroscopy[40] and in previous QENS measurements,[11] where the onset of the sharp decrease in dehydration occurred ~1−2 K above T_{cp}. Above T_{cp}, a significant fraction of hydration water remains, which decreases gradually with increasing temperature. This regime extends as far as ~10 K above T_{cp}. A small fraction (~0.15) remains even at 55.2 °C. These results are consistent with the notion that at atmospheric pressure PNIPAM chains do not dehydrate completely at T_{cp}, and the majority of the hydrophilic amide groups remain hydrogen bonded with water rather than forming intra- or interchain hydrogen bonds.[24] Thus, the dehydration is mainly related to the release of water from the hydrophobic groups.
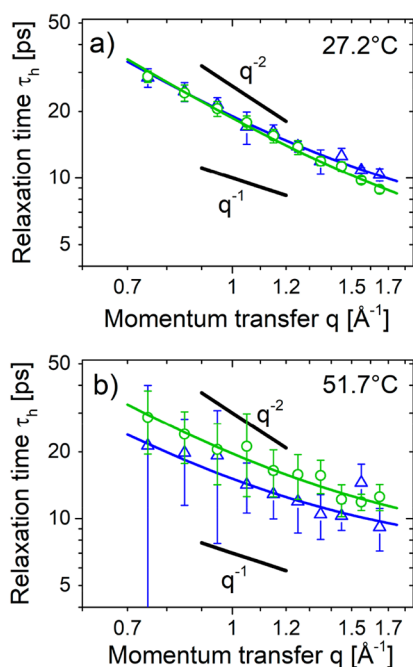
In the one-phase region at 130 MPa, the relative population of hydration water is similar to the one at atmospheric pressure. However, at T_{cp}, no sharp transition is observed, rather the relative population of hydration water decreases smoothly over the entire temperature range measured, i.e., up to 55.2 °C, where the value is ~0.15. From this point of view, the phase transition is different at both pressures.

This difference in behavior at T_{cp} at low and high pressure is consistent with results from our previous study using Raman spectroscopy, where the frequency of the stretching vibrations of the CH$_3$ groups (present in the isopropyl groups) was investigated.[40] It changes abruptly at atmospheric pressure, but only gradually and over a large temperature range at high pressure, even though aggregates are formed within 0.1 K above T_{cp} in both cases. Furthermore, differential scanning calorimetry (DSC) measurements showed a broadening of the heat capacity peak at high pressure, implying that dehydration occurs on a larger temperature range than at atmospheric pressure.[79]

The relative population of bulk water increases sharply at atmospheric pressure and gradually at 130 MPa, as is observed from the increase of both the diffusive and the local part. Thus, the hydration water that is released from the chains at T_{cp} adds to the bulk water phase.

The elastic line strength $C_{q,el}$ is depicted in dependence on temperature in Figure 6b for $q = 1.65$ Å^{-1}. It increases with temperature, both at atmospheric pressure and at 130 MPa. At atmospheric pressure, it stays constant below T_{cp} and increases sharply at T_{cp}. This increase may be due to both trapped water inside the polymer-rich domains and immobilized groups of the polymer. A certain amount of the hydration water above T_{cp} thus stays close to the chains rather than joining the bulk water phase. At high pressure, the elastic line strength increases gradually at T_{cp}, which confirms that in this case the phase transition spans a broad temperature range.

Relaxation Times of Hydration Water. The dependence of the relaxation time of the hydration water, τ_h, on the momentum transfer q reveals the signature of the hydration water as well as its changes at the phase transition. Figure 7a shows the q dependence of τ_h for both 0.1 and 130 MPa at 27.2 °C, i.e., in the one-phase region. For both pressures, a behavior between q^{-1} and q^{-2} is observed, which becomes shallower with increasing q. For purely diffusive processes, $\tau_h \propto q^{-2}$ is expected, and this behavior is nearly achieved in the one-phase state at both pressures (Figure 7a). In the two-phase state, the dependence is weaker, and in the entire q range investigated, τ_h is higher at 130 MPa than at atmospheric pressure.

Figure 7. q dependence of the relaxation time of hydration water, τ_h, in the one-phase region at 27.2 °C (a) and in the two-phase region at 51.7 °C (b). Blue triangles: 0.1 MPa; green circles: 130 MPa; full lines: fits of eq 6: 0.1 MPa (blue lines) and 130 MPa (green lines).

Figure 8. Results obtained from fits of the isotropic jump model (eq 6) to $\tau_h(q)$ (filled symbols) and to $\tau_d(q)$ (open symbols) at 0.1 MPa (blue triangles) and 130 MPa (green circles) in dependence on temperature: (a) residence times, $\tau_{0,i}$, (b) apparent jump lengths, l_i, and (c) diffusion coefficients, D_i.

The behavior of the hydration water of PNIPAM is thus fundamentally different from the one observed in proteins, namely, diffusion in a restricted area or volume or subdiffusive behavior, which manifests itself in a stronger q dependence than $\tau_h \propto q^{-2}$.[12,54] The weaker dependence may have different origins. For instance, it may point to superdiffusive behavior.[12,80] However, superdiffusive behavior would require an anisotropic force acting on the water molecules, which in the present case is unlikely. Furthermore, a change of the behavior is observed with varying q. The situation appears thus more complex. In analogy with the diffusive process of pure water, the isotropic jump model (eq 6) is used to describe the dynamic behavior of the hydration water. It comprises a residence time, $\tau_{0,h}$, as well as an apparent jump length, l_h. The fits, also shown in Figure 7a, are in excellent agreement with the data over the entire q range. In the two-phase region, shown in Figure 7b for 51.7 °C, the observed slope is lower than in the one-phase region. Also in this case, the q dependence of τ_h can be modeled by the isotropic jump model. We note that since neither a q^{-2} at low q values nor a constant value at high q values is fully reached, the determination of both D_h and $\tau_{0,h}$ rely on extrapolation. Furthermore, because of the small relative population of hydration water in the two-phase region, the uncertainties of τ_h are large.

Figure 8 compares the results of the fits of the q dependence of τ_h and of τ_d with the isotropic jump model. The residence time, $\tau_{0,i}$, i.e., the time a water molecule stays in place and performs a local motion, is shown in Figure 8a. At atmospheric pressure below T_{cp}, the residence time of the hydration water, $\tau_{0,h}$, is ~5 ps, independent of temperature. This is a factor of ~10 larger than the residence time of bulk water at the same conditions ($\tau_{0,d}$, also shown in Figure 8a). One reason for this increase may be that in the PNIPAM solution the number of vacant jumping sites around the hydration water molecules is
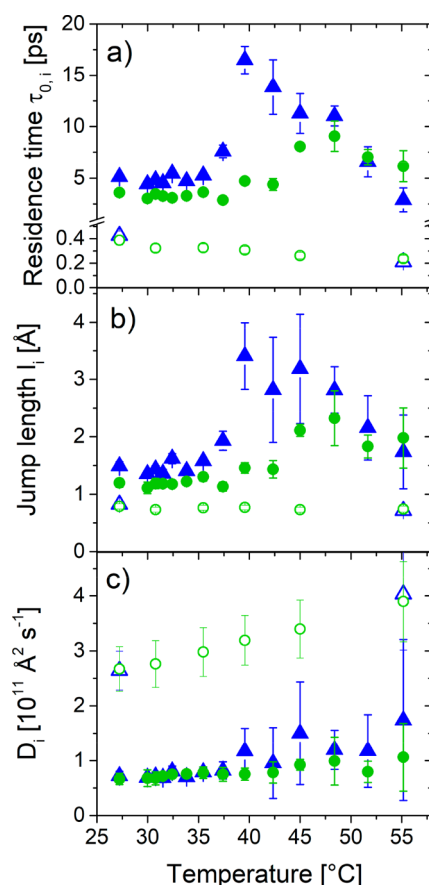
low. The local environment of the hydration water is dominated by nearby polymeric groups. Around the hydrophobic groups, the bond strength of the water molecules among each other may be similar to the one of the bulk water molecules.[10,81] However, the number of accessible sites for jumps is reduced by the presence of the hydrophobic groups, thus leading to an increased residence time. This increase does not exceed a factor of 2 in dilute solutions.[10,81] For the hydrophilic groups, the strong hydrogen bonds between water and the hydrophilic groups constrain the motion of hydration water further. Breaking the initial hydrogen bond upon jumping requires an activation energy, which hinders the diffusion with retardation factors up to 4 in dilute solutions.[82] The large difference in residence time between bulk water and hydration water in the one-phase region must therefore be caused by concentration effects: Every hydration water molecule is shielded from the bulk water phase on more than one side; i.e., several polymer groups are on average involved in the binding of one hydration water molecule.

In the one-phase region at 130 MPa, $\tau_{0,h}$ is significantly lower than at 0.1 MPa, namely ~3 ps. In contrast, the relative populations of hydration water in the one-phase region are similar at both pressures. Thus, at high pressure, the hydration water is distributed differently on the polymeric chains. The shorter residence time at high pressure reflects a weaker constraint of hydration water motion than at atmospheric pressure. The effect of pressure on the individual bond

strength is very small in the investigated pressure range and has thus only a minor effect.[83,84] It can be concluded that the polar groups are less hydrated, in favor of the hydrophobic groups, which are more hydrated at high pressure. Enhanced hydrophobic hydration of macromolecules at high pressure was also inferred with spectroscopic methods.[39] From molecular dynamics simulations, it was concluded that the compressibility of hydration water around hydrophobic groups is much larger than the one of bulk water and the one of hydration water around hydrophilic groups.[34,36,37]

At 0.1 MPs, $\tau_{0,h}$ increases from ∼7.5 to ∼16.5 ps at ∼37 °C, i.e., above T_{cp}. This increase coincides with the sharp decrease in the relative population of the hydration water (Figure 6a) and with the sharp increase of the elastic line strength (Figure 6b). The observed distribution of relaxation times of the hydration water in the soluble phase at both pressures implies that bonds of different strengths between hydration water and the chains exist. The increase in $\tau_{0,h}$ may be a result of two mechanisms: First, weakly bound hydration water is released from the chains at T_{cp}, and only strongly bound hydration water remains, which is characterized by a high residence time. Second, both strongly and weakly bound hydration water are released from the chains in significant amounts at T_{cp}, and the remaining population is increasingly hindered in its motion due to the chain collapse. The latter scenario is also consistent with the increase of the elastic line strength at T_{cp}. A combination of both effects may, however, also be possible. This result is in agreement with the current understanding of the phase-separation process of PNIPAM at atmospheric pressure: At T_{cp}, the collapse of the chains causes a strong dehydration of their hydrophobic groups. The subsequent aggregation[24,40] leads to trapping of water molecules,[11,85] which results in longer residence times. In contrast, according to spectroscopy measurements,[24,76,85] the hydrophilic amide groups stay hydrated above T_{cp}.

Moreover, at 130 MPa, an increase in $\tau_{0,h}$ with temperature is seen just above T_{cp}. The increase is more gradual (extending to ∼10 K above T_{cp}) with a weaker temperature dependence. Because the relative population of hydration water decreases gradually in the two-phase region, the increase in $\tau_{0,h}$ is most likely caused by an increased hindrance of the remaining hydration water in the two-phase region. This would be consistent with the increase in the elastic line strength, albeit to a lesser extent than at atmospheric pressure. As was suggested previously,[34,86] at high pressures, the dissociation of close hydrophobic contacts is favored. The process of hydrophobic collapse therefore appears impeded at high pressure and presumably extends to about 10 K above T_{cp}.

At temperatures far above T_{cp}, a decrease in $\tau_{0,h}$ is observed at atmospheric pressure (Figure 8a). The relative population of hydration water and the elastic line strength in the two-phase region are constant; thus, the same amount of water molecules is considered. The faster relaxation times of the hydration water can therefore be attributed to structural changes in the polymer-rich phase with increasing temperature. Rearrangements in the system allow strongly hindered water to relax, possibly by forming water pockets inside the polymer-rich phase where water accumulates. This loosening of hydration water is not observed at high pressure, where $\tau_{0,h}$ stays constant far above T_{cp}. Thus, structural changes play a much weaker role.

The apparent jump length of the hydration water, l_h, is presented in Figure 8b. For both pressures, it shows similar trends as the residence time. The apparent jump length is a measure of the spatial range of the motion of water molecules as well as their dynamics[9] and may thus be expected to correlate with the residence time, as is observed. Compared to the apparent jump length of bulk water, l_d, the values in the one-phase region are slightly larger, presumably due to a less dense packing of water close to the chains than in bulk water.

The diffusion coefficient of the hydration water, D_h, calculated from the residence time and the apparent jump length, is shown in Figure 8c. In the one-phase region, D_h is approximately equal for both pressures. At 27.2 °C, it is ∼7 × 10^{10} Å^2 s^{-1}, which is a factor of ∼4 smaller than the value of pure water at the same temperature. With increasing temperature, a slight increase in D_h is observed for both pressures, which is most probably caused by the enhanced thermal energy. Above T_{cp}, an increase in D_h is observed, which is stronger at atmospheric pressure than at 130 MPa, where it has a similar slope as in the one-phase region. However, the uncertainties are large. Possibly, water pockets inside the polymer-rich domains at atmospheric pressure provide more room for diffusion than the homogeneous aggregates at high pressure.

Intensity of the Elastic Line in Dependence of Temperature and Pressure. The elastic component of the dynamic structure factor gives information about very slowly moving structures and has the shape of the instrument resolution function. Apart from the dynamics of the hydration water, the dynamics of the polymeric chains are also accessible, namely from the q dependence of the elastic line strength (Figure 9a). Its intensity arises from processes that are too
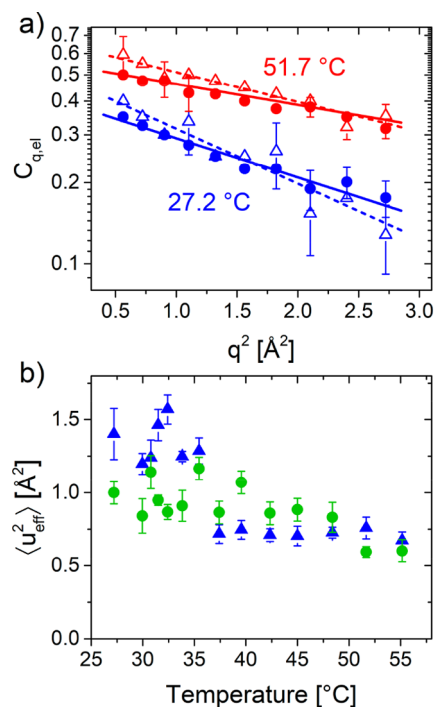
Figure 9. (a) Elastic line strength in dependence on q^2 at 27.2 °C (blue symbols) and 51.7 °C (red symbols) at 0.1 MPa (open triangles) and 130 MPa (closed circles). Lines: fits of eq 11 at 27.2 °C (blue lines) and 51.7 °C (red lines) at 0.1 MPa (dashed lines) and 130 MPa (solid lines). (b) Temperature dependence of the effective mean-square displacement $\langle u_{eff}^2 \rangle$ of the dynamics of PNIPAM at 0.1 MPa (blue triangles) and 130 MPa (green circles).

slow to be spectrally resolved, which are in this case, mainly motions of the polymer. However, also water trapped in the polymer-rich phase in the two-phase region may contribute to the elastic line strength. Figure 9a shows the elastic line strength in a logarithmic representation in dependence on q^2 for both pressures in the one-phase and in the two-phase region. In all cases, it follows a straight line, which allows a description using the Debye−Waller factor:[55]

$$C_{q,el} \sim \exp\left(\frac{-\langle u_{eff}^2 \rangle q^2}{3}\right)$$

$$(11)$$

with $\langle u_{eff}^2 \rangle$ the mean-square displacement of the observed process. As multiple processes may contribute to the elastic line, the determined mean-square displacement is an effective one.

Figure 9b shows $\langle u_{eff}^2 \rangle$ in dependence on temperature at both pressures. At atmospheric pressure, $\langle u_{eff}^2 \rangle$ decreases sharply at T_{cp} from ~1.3 to ~0.7 Å^2, which reflects the sudden collapse of the chains at T_{cp}. In the one-phase region, translational motion of the polymer segments is rather free, and local changes in chain conformation may also contribute to the elastic line strength, resulting in a large effective mean-square displacement. In the two-phase region at 0.1 MPa, the chains are collapsed and densely packed, but still, the mean-square displacement is finite. Translational motion of the polymer segments is only possible if neighboring segments also move and is thus strongly constrained. Vibrational motions, however, require only little volume and are still possible. Furthermore, the observed displacement may involve rotational motions of (predominantly) the methyl groups,[87] as previously observed in dry as well as in hydrated protein samples.[56,88]

At high pressure, $\langle u_{eff}^2 \rangle$ decreases gradually from ~1 to ~0.6 Å^2 without a sharp change at T_{cp}; however, the data are rather scattered. This confirms the observations from the behavior of the hydration water: The conformation of the chains changes gradually from a swollen and thus mobile state to a collapsed and immobile state. The most notable difference with respect to the measurement at atmospheric pressure is the significantly lower value of $\langle u_{eff}^2 \rangle$ in the one-phase region. It shows that the motion of the chains is more restricted at high pressure. We conclude that the altered hydration state at high pressure causes chain stiffening. Possibly, the enhanced hydrophobic hydration of the side groups causes a certain degree of steric hindrance to conformational changes of the polymer, thereby restricting translational motion. Furthermore, the reduced hydration of hydrophilic groups, evident from the different values of $\tau_{0,h}$ at both pressures (Figure 8a), may allow the formation of N−H···O=C bonds between nearby monomers, stiffening the chains. A lower value of $\langle u_{eff}^2 \rangle$ in the one-phase region at high pressure was also observed previously and confirmed using DLS measurements.[25]

CONCLUSIONS

In the present work, the dynamic behavior of hydration water in an aqueous PNIPAM solution is investigated in dependence on temperature and pressure using quasi-elastic neutron scattering. It is found that the dynamics of hydration water can be described by the jump diffusion model.

In the one-phase region, i.e., below T_{cp}, the relative population of hydration water is equal at pressures of 0.1 and 130 MPa and decreases weakly with increasing temper-

ature at both pressures. However, at 130 MPa, the residence time becomes shorter, and the hydration water is more weakly bound, pointing to enhanced hydrophobic hydration at the expense of the hydration of hydrophilic groups. At the cloud point, a sharp decrease in the relative population of hydration water is observed at atmospheric pressure. The remaining hydration water is, on average, more strongly hindered than the hydration water in the one-phase region. At 130 MPa, the relative population of hydration water decreases gradually, and hydration water gets increasingly hindered, resulting in a longer residence time. Both effects are weaker and more gradual than at atmospheric pressure, where water is trapped in the polymer-rich domains. Deep in the two-phase region at atmospheric pressure, a loosening of hydration water due to structural relaxation of the polymer-rich domains is observed. At 130 MPa, these structural changes do not occur. This picture is consistent with our previous Raman spectroscopy measurements on aqueous PNIPAM solutions.[40] At high pressure, the dehydration of the CH$_3$ groups at the side groups of PNIPAM occurs gradually (extending to at least 10 K above T_{cp}) and to a lesser extent than at atmospheric pressure.

Moreover, the effective mean-square displacement of the polymer chains is determined from the strength of the elastic line, which is due to translational, vibrational, and rotational displacements. At 0.1 MPa, a sharp decrease of the effective mean-square displacement is observed at T_{cp}, whereas at 130 MPa, it decreases gradually. In the one-phase region, translation due to changes in the local chain conformation is possible because of the strong hydration of the chains. In the two-phase region, mostly vibrational and rotational processes are observed. It is also evident that the phase transition occurs more gradual at high pressure. Finally, the lower value of the mean-square displacement at high pressure in the soluble phase suggests that the altered hydration state at high pressure leads to chain stiffening

In summary, a detailed investigation of the dynamics of the hydration water in aqueous PNIPAM solutions in dependence on temperature and pressure has been presented. The wide range of accessible energy and momentum transfers allows distinguishing the relaxation of hydration water around PNIPAM chains and various relaxation processes in bulk water. The findings concerning the dynamics of hydration water in this model responsive polymer point to new opportunities for studies of more complex systems using QENS.

■ ASSOCIATED CONTENT

ⓈSupporting Information

The Supporting Information is available free of charge on the ACS Publications website at DOI: 10.1021/acs.macro-mol.8b02708.

> Determination of cloud points; comparison of fitting models; example fits in the entire q range (PDF)

■ AUTHOR INFORMATION

Corresponding Authors
*(C.M.P.) E-mail papadakis@tum.de.
*(A.S.) E-mail alfons.schulte@ucf.edu.
ORCID ⓘ
Alfons Schulte: 0000-0003-0824-8572
Christine M. Papadakis: 0000-0002-7098-3458

■ REFERENCES

(1) Bellissent-Funel, M.-C.; Hassanali, A.; Havenith, M.; Henchman, R.; Pohl, P.; Sterpone, F.; van der Spoel, D.; Xu, Y.; Garcia, A. E. Water Determines the Structure and Dynamics of Proteins. *Chem. Rev.* **2016**, *116*, 7673−7697.

(2) Laage, D.; Elsaesser, T.; Hynes, J. T. Water Dynamics in the Hydration Shells of Biomolecules. *Chem. Rev.* **2017**, *117*, 10694−10725.

(3) Aseyev, V.; Tenhu, H.; Winnik, F. M. Non-Ionic Thermoresponsive Polymers in Water. *Adv. Polym. Sci.* **2010**, *242*, 29−89.

(4) Pissis, P.; Kyritsis, A. Hydration Studies in Polymer Hydrogels. *J. Polym. Sci., Part B: Polym. Phys.* **2013**, *51*, 159−175.

(5) Kojima, H. Studies on the Phase Transition of Hydrogels and Aqueous Solutions of Thermoresponsive Polymers. *Polym. J.* **2018**, *50*, 411−418.

(6) Singwi, K. S.; Sjölander, A. Diffusive Motions in Water and Cold Neutron Scattering. *Phys. Rev.* **1960**, *119*, 863−871.

(7) Teixeira, J.; Bellissent-Funel, M.-C.; Chen, S. H.; Dianoux, A. J. Experimental Determination of the Nature of Diffusive Motions of Water Molecules at Low Temperatures. *Phys. Rev. A: At., Mol., Opt. Phys.* **1985**, *31*, 1913−1917.

(8) Laage, D. Reinterpretation of the Liquid Water Quasi-Elastic Neutron Scattering Spectra Based on a Nondiffusive Jump Reorientation Mechanism. *J. Phys. Chem. B* **2009**, *113*, 2684−2687.

(9) Qvist, J.; Schober, H.; Halle, B. Structural Dynamics of Supercooled Water from Quasielastic Neutron Scattering and Molecular Simulations. *J. Chem. Phys.* **2011**, *134*, 144508.

(10) Laage, D.; Stirnemann, G.; Sterpone, F.; Rey, R.; Hynes, J. T. Reorientation and Allied Dynamics in Water and Aqueous Solutions. *Annu. Rev. Phys. Chem.* **2011**, *62*, 395−416.

(11) Philipp, M.; Kyriakos, K.; Silvi, L.; Lohstroh, W.; Petry, W.; Krüger, J. K.; Papadakis, C. M.; Müller-Buschbaum, P. From Molecular Dehydration to Excess Volumes of Phase-Separating PNIPAM Solutions. *J. Phys. Chem. B* **2014**, *118*, 4253−4260.

(12) Tan, P.; Liang, Y.; Xu, Q.; Mamontov, E.; Li, J.; Xing, X.; Hong, L. Gradual Crossover from Subdiffusion to Normal Diffusion: A Many-Body Effect in Protein Surface Water. *Phys. Rev. Lett.* **2018**, *120*, 248101.

(13) Settles, M.; Doster, W. Anomalous Diffusion of Adsorbed Water: A Neutron Scattering Study of Hydrated Myoglobin. *Faraday Discuss.* **1996**, *103*, 269−279.

(14) Rocchi, C.; Bizzarri, A. R.; Cannistraro, S. Water Dynamical Anomalies Evidenced by Molecular-Dynamics Simulations at the Solvent-Protein Interface. *Phys. Rev. E: Stat. Phys., Plasmas, Fluids, Relat. Interdiscip. Top.* **1998**, *57*, 3315−3325.

(15) Stirnemann, G.; Sterpone, F.; Laage, D. Dynamics of Water in Concentrated Solutions of Amphiphiles: Key Roles of Local Structure and Aggregation. *J. Phys. Chem. B* **2011**, *115*, 3254−3262.

(16) Capponi, S.; Arbe, A.; Cerveny, S.; Busselez, R.; Frick, B.; Embs, J. P.; Colmenero, J. Quasielastic Neutron Scattering Study of Hydrogen Motions in an Aqueous Poly(Vinyl Methyl Ether) Solution. *J. Chem. Phys.* **2011**, *134*, 204906.

(17) Laurati, M.; Sotta, P.; Long, D. R.; Fillot, L.-A.; Arbe, A.; Alegría, A.; Embs, J. P.; Unruh, T.; Schneider, G. J.; Colmenero, J. Dynamics of Water Absorbed in Polyamides. *Macromolecules* **2012**, *45*, 1676−1687.

(18) Busselez, R.; Arbe, A.; Cerveny, S.; Capponi, S.; Colmenero, J.; Frick, B. Component Dynamics in Polyvinylpyrrolidone Concentrated Aqueous Solutions. *J. Chem. Phys.* **2012**, *137*, 084902.

(19) Malo de Molina, P.; Alvarez, F.; Frick, B.; Wildes, A.; Arbe, A.; Colmenero, J. Investigation of the Dynamics of Aqueous Proline Solutions Using Neutron Scattering and Molecular Dynamics Simulations. *Phys. Chem. Chem. Phys.* **2017**, *19*, 27739−27754.

(20) Halperin, A.; Kröger, M.; Winnik, F. M. Poly(N-isopropylacrylamide) Phase Diagrams: Fifty Years of Research. *Angew. Chem., Int. Ed.* **2015**, *54*, 15342−15367.

(21) Abbott, L. J.; Tucker, A. K.; Stevens, M. J. Single Chain Structure of a Poly(N-isopropylacrylamide) Surfactant in Water. *J. Phys. Chem. B* **2015**, *119*, 3837−3845.

(22) Okada, Y.; Tanaka, F. Cooperative Hydration, Chain Collapse, and Flat LCST Behavior in Aqueous Poly(N-isopropylacrylamide) Solutions. *Macromolecules* **2005**, *38*, 4465−4471.

(23) Deshmukh, S. A.; Sankaranarayanan, S. K. R. S.; Suthar, K.; Mancini, D. C. Role of Solvation Dynamics and Local Ordering of Water in Inducing Conformational Transitions in Poly(N-isopropylacrylamide) Oligomers through the LCST. *J. Phys. Chem. B* **2012**, *116*, 2651−2663.

(24) Maeda, Y.; Higuchi, T.; Ikeda, I. Change in Hydration State During the Coil-Globule Transition of Aqueous Solutions of Poly(N-isopropylacrylamide) as Evidenced by FTIR Spectroscopy. *Langmuir* **2000**, *16*, 7503−7509.

(25) Osaka, N.; Shibayama, M.; Kikuchi, T.; Yamamuro, O. Quasi-Elastic Neutron Scattering Study on Water and Polymer Dynamics in Thermo/Pressure Sensitive Polymer Solutions. *J. Phys. Chem. B* **2009**, *113*, 12870−12876.

(26) Füllbrandt, M.; Ermilova, E.; Asadujjaman, A.; Hölzel, R.; Bier, F. F.; von Klitzing, R.; Schönhals, A. Dynamics of Linear Poly(N-isopropylacrylamide) in Water Around the Phase Transition Investigated by Dielectric Relaxation Spectroscopy. *J. Phys. Chem. B* **2014**, *118*, 3750−3759.

(27) Cho, E. C.; Lee, J.; Cho, K. Role of Bound Water and Hydrophobic Interaction in Phase Transition of Poly(N-isopropylacrylamide) Aqueous Solution. *Macromolecules* **2003**, *36*, 9929−9934.

(28) Ono, Y.; Shikata, T. Contrary Hydration Behavior of N-isopropylacrylamide to its Polymer, P(NIPAm), with a Lower Critical Solution Temperature. *J. Phys. Chem. B* **2007**, *111*, 1511−1513.

(29) Otake, K.; Karaki, R.; Ebina, T.; Yokoyama, C.; Takahashi, S. *Macromolecules* **1993**, *26*, 2194−2197.

(30) Kunugi, S.; Yamazaki, Y.; Takano, K.; Tanaka, N.; Akashi, M. Effects of Ionic Additives and Ionic comonomers on the Temperature and Pressure Responsive Behavior of Thermoresponsive Polymers in Aqueous Solutions. *Langmuir* **1999**, *15*, 4056−4061.

(31) Shibayama, M.; Isono, K.; Okabe, S.; Karino, T.; Nagao, M. SANS Study on Pressure-Induced Phase Separation of Poly(N-isopropylacrylamide) Aqueous Solutions and Gels. *Macromolecules* **2004**, *37*, 2909−2918.

(32) Ebeling, B.; Eggers, S.; Hendrich, M.; Nitschke, A.; Vana, P. Flipping the Pressure- and Temperature-Dependent Cloud-Point Behavior in the Cononsolvency System of Poly(N-isopropylacrylamide) in Water and Ethanol. *Macromolecules* **2014**, *47*, 1462−1469.

(33) Niebuur, B.-J.; Chiappisi, L.; Zhang, X.; Jung, F.; Schulte, A.; Papadakis, C. M. Formation and Growth of Mesoglobules in Aqueous Poly(N-isopropylacrylamide) Solutions Revealed with Kinetic Small-Angle Neutron Scattering and Fast Pressure Jumps. *ACS Macro Lett.* **2018**, *7*, 1155−1160.

(34) Ghosh, T.; García, A. E.; Garde, S. Molecular Dynamics Simulations of Pressure Effects on Hydrophobic Interactions. *J. Am. Chem. Soc.* **2001**, *123*, 10997−11003.

(35) Dadarlat, V. M.; Post, C. B. Decomposition of Protein Experimental Compressibility into Intrinsic and Hydration Shell Contributions. *Biophys. J.* **2006**, *91*, 4544−4554.

(36) Smolin, N.; Winter, R. A Molecular Dynamics Simulation of Snase and its Hydration shell at High Temperature and High Pressure. *Biochim. Biophys. Acta, Proteins Proteomics* **2006**, *1764*, 522–534.

(37) Sarupria, S.; Garde, S. Quantifying Water Density Fluctuations and Compressibility of Hydration Shells of Hydrophobic Solutes and Proteins. *Phys. Rev. Lett.* **2009**, *103*, 037803.

(38) Grigera, J. R.; McCarthy, A. N. The Behavior of the Hydrophobic Effect under Pressure and Protein Denaturation. *Biophys. J.* **2010**, *98*, 1626–1631.

(39) Meersman, F.; Wang, J.; Wu, Y.; Heremans, K. Pressure Effect on the Hydration Properties of Poly(*N*-isopropylacrylamide) in Aqueous Solution Studied by FTIR Spectroscopy. *Macromolecules* **2005**, *38*, 8923–8928.

(40) Niebuur, B.-J.; Claude, K.-L.; Pinzek, S.; Cariker, C.; Raftopoulos, K. N.; Pipich, V.; Appavou, M.-S.; Schulte, A.; Papadakis, C. M. Pressure-Dependence of Poly(*N*-isopropylacrylamide) Mesoglobule Formation in Aqueous Solution. *ACS Macro Lett.* **2017**, *6*, 1180–1185.

(41) Mochizuki, K.; Sumi, T.; Koga, K. Driving Forces for the Pressure-Induced Aggregation of Poly(*N*-isopropylacrylamide) in Water. *Phys. Chem. Chem. Phys.* **2016**, *18*, 4697.

(42) Arbe, A.; Malo de Molina, P.; Alvarez, F.; Frick, B.; Colmenero, J. Dielectric Susceptibilities of Liquid Water: Microscopic Insights from Coherent and Incoherent Neutron Scattering. *Phys. Rev. Lett.* **2016**, *117*, 185501.

(43) Sears, V. F. Neutron Scattering Lengths and Cross Sections. *Neutron News* **1992**, *3*, 26–37.

(44) Unruh, T.; Neuhaus, J.; Petry, W. The High-Resolution Time-of-Flight Spectrometer TOFTOF. *Nucl. Instrum. Methods Phys. Res., Sect. A* **2007**, *580*, 1414–1422.

(45) Lohstroh, W.; Evenson, Z. TOFTOF: Cold Neutron Time-of-Flight Spectrometer. *Journal of large-scale research facilities JLSRF* **2015**, *1*, A15.

(46) Appavou, M.-S.; Busch, S.; Doster, W.; Gaspar, A.; Unruh, T. The Influence of 2 kbar Pressure on the Global and Internal Dynamics of Human Hemoglobin Observed by Quasielastic Neutron Scattering. *Eur. Biophys. J.* **2011**, *40*, 705–714.

(47) Arnold, O.; Bilheux, J. C.; Borreguero, J. M.; Buts, A.; Campbell, S. I.; Chapon, L.; Doucet, M.; Draper, N.; Ferraz Leal, R.; Gigg, M. A.; Lynch, V. E.; Markvardsen, A.; Mikkelson, D. J.; Mikkelson, R. L.; Miller, R.; Palmen, K.; Parker, P.; Passos, G.; Perring, T. G.; Peterson, P. F.; Ren, S.; Reuter, M. A.; Savici, A. T.; Taylor, J. W.; Taylor, R. J.; Tolchenov, R.; Zhou, W.; Zikovsky, J. Mantid — Data Analysis and Visualization Package for Neutron Scattering and μ SR Experiments. *Nucl. Instrum. Methods Phys. Res., Sect. A* **2014**, *764*, 156–166.

(48) Shibayama, M.; Morimoto, M.; Nomura, M. Phase Separation Induced Mechanical Transition of Poly(*N*-isopropylacrylamide)/Water Isochore Gels. *Macromolecules* **1994**, *27*, 5060–5066.

(49) Shiraga, K.; Naito, H.; Suzuki, T.; Kondo, N.; Ogawa, Y. Hydration and Hydrogen Bond Network of Water during the Coil-to-Globule Transition in Poly(*N*-isopropylacrylamide) Aqueous Solution at Cloud Point Temperature. *J. Phys. Chem. B* **2015**, *119*, 5576–5587.

(50) Kyriakos, K.; Philipp, M.; Silvi, L.; Lohstroh, W.; Petry, W.; Müller-Buschbaum, P.; Papadakis, C. M. Solvent Dynamics in Solutions of PNIPAM in Water/Methanol Mixtures — A Quasi-Elastic Neutron Scattering Study. *J. Phys. Chem. B* **2016**, *120*, 4679–4688.

(51) Sokolov, A. P.; Grimm, H.; Kisliuk, A.; Dianoux, A. J. Slow Relaxation Process in DNA. *J. Biol. Phys.* **2001**, *27*, 313–327.

(52) Bizzarri, A. R.; Cannistraro, S. Molecular Dynamics of Water at the Protein-Solvent Interface. *J. Phys. Chem. B* **2002**, *106*, 6617–6633.

(53) Doster, W.; Gebhardt, R. High Pressure-Unfolding of Myoglobin Studied by Dynamic Neutron Scattering. *Chem. Phys.* **2003**, *292*, 383–387.

(54) Perticaroli, S.; Ehlers, G.; Stanley, C. B.; Mamontov, E.; O'Neill, H.; Zhang, Q.; Cheng, X.; Myles, D. A. A.; Katsaras, J.; Nickels, J. D. Description of Hydration Water in Protein (Green Fluorescent Protein) Solution. *J. Am. Chem. Soc.* **2017**, *139*, 1098–1105.

(55) Doster, W.; Cusack, S.; Petry, W. Dynamic Instability of Liquidlike Motions in a Globular Protein Observed by Inelastic Neutron Scattering. *Phys. Rev. Lett.* **1990**, *65*, 1080–1083.

(56) Roh, J. H.; Curtis, J. E.; Azzam, S.; Novikov, V. N.; Peral, I.; Chowdhuri, Z.; Gregory, R. B.; Sokolov, A. P. Influence of Hydration on the Dynamics of Lysozyme. *Biophys. J.* **2006**, *91*, 2573–2588.

(57) Bergman, R. General Susceptibility Functions for Relaxations in Disordered Systems. *J. Appl. Phys.* **2000**, *88*, 1356–1365.

(58) Fåk, B.; Dorner, B. Phonon Line Shapes and Excitation Energies. *Phys. B* **1997**, *234–236*, 1107–1108.

(59) Ohmine, I. Liquid Water Dynamics: Collective Motions, Fluctuations, and Relaxation. *J. Phys. Chem.* **1995**, *99*, 6767–6776.

(60) Walrafen, G. W.; Chu, Y. C. Linearity Between Structural Correlation Length and Correlated-Proton Raman Intensity from Amorphous Ice and Supercooled Water up to Dense Supercritical Steam. *J. Phys. Chem.* **1995**, *99*, 11225–11229.

(61) Wan, Q.; Spanu, L.; Galli, G. A.; Gygi, F. Raman Spectra of Liquid Water from Ab Initio Molecular Dynamics: Vibrational Signatures of Charge Fluctuations in the Hydrogen Bond Network. *J. Chem. Theory Comput.* **2013**, *9*, 4124–4130.

(62) Russo, D.; Laloni, A.; Filabozzi, A.; Heyden, M. Pressure Effects on Collective Density Fluctuations in Water and Protein Solutions. *Proc. Natl. Acad. Sci. U. S. A.* **2017**, *114*, 11410–11415.

(63) Ghugare, S. V.; Chiessi, E.; Telling, M. T. F.; Deriu, A.; Gerelli, Y.; Wuttke, J.; Paradossi, G. Structure and Dynamics of a Thermoresponsive Microgel around its Volume Phase Transition Temperature. *J. Phys. Chem. B* **2010**, *114*, 10285–10293.

(64) Chen, S.-H.; Gallo, P.; Sciortino, F.; Tartaglia, P. Molecular-Dynamics Study of Incoherent Quasielastic Neutron-Scattering Spectra of Supercooled Water. *Phys. Rev. E: Stat. Phys., Plasmas, Fluids, Relat. Interdiscip. Top.* **1997**, *56*, 4231–4243.

(65) Cunsolo, A.; Orecchini, A.; Petrillo, C.; Sacchetti, F. Quasielastic Neutron Scattering Investigation of the Pressure Dependence of Molecular Motions in Liquid Water. *J. Chem. Phys.* **2006**, *124*, 084503.

(66) Bove, L. E.; Klotz, S.; Strässle, T.; Koza, M.; Teixeira, J.; Saitta, A. M. Translational and Rotational Diffusion in Water in the Gigapascal Range. *Phys. Rev. Lett.* **2013**, *111*, 185901.

(67) Wang, J. H. Self-Diffusion Coefficients of Water. *J. Phys. Chem.* **1965**, *69*, 4412.

(68) Yoshida, K.; Matubayasi, N.; Nakahara, M. Self-Diffusion Coefficients for Water and Organic Solvents at High Temperatures along the Coexistence Curve. *J. Chem. Phys.* **2008**, *129*, 214501.

(69) Kikuchi, T.; Nakajima, K.; Ohira-Kawamura, S.; Inamura, Y.; Yamamuro, O.; Kofu, M.; Kawakita, Y.; Suzuya, K.; Nakamura, M.; Arai, M. Mode-Distribution Analysis of Quasielastic Neutron Scattering and Application to Liquid Water. *Phys. Rev. E* **2013**, *87*, 062314.

(70) Harris, K. R.; Woolf, L. A. Pressure and Temperature Dependence of the Self Diffusion Coefficient of Water and Oxygen-18 Water. *J. Chem. Soc., Faraday Trans. 1* **1980**, *76*, 377–385.

(71) Yeh, Y.-L.; Mou, C.-Y. Orientational Relaxation Dynamics of Liquid Water Studied by Molecular Dynamics Simulation. *J. Phys. Chem. B* **1999**, *103*, 3699–3705.

(72) Yada, H.; Nagai, M.; Tanaka, K. Origin of the Fast Relaxation Component of Water and Heavy Water Revealed by Terahertz Time-Domain Attenuated Total Reflection Spectroscopy. *Chem. Phys. Lett.* **2008**, *464*, 166–170.

(73) Zasetsky, A. Y. Dielectric Relaxation in Liquid Water: Two Fractions or Two Dynamics? *Phys. Rev. Lett.* **2011**, *107*, 117601.

(74) Popov, I.; Ishai, P. B.; Khamzin, A.; Feldman, Y. The Mechanism of the Dielectric Relaxation in Water. *Phys. Chem. Chem. Phys.* **2016**, *18*, 13941–13953.

(75) Sun, B.; Lin, Y.; Wu, P.; Siesler, H. W. A FTIR and 2D-IR Spectroscopic Study on the Microdynamics Phase Separation Mechanism of the Poly(*N*-isopropylacrylamide) Aqueous Solution. *Macromolecules* **2008**, *41*, 1512–1520.

(76) Ahmed, Z.; Gooding, E. A.; Pimenov, K. V.; Wang, L.; Asher, S. A. UV Resonance Raman Determination of Molecular Mechanism of Poly(*N*-isopropylacrylamide) Volume Phase Transition. *J. Phys. Chem. B* **2009**, *113*, 4248−4256.

(77) Futscher, M. H.; Philipp, M.; Müller-Buschbaum, P.; Schulte, A. The Role of Backbone Hydration of Poly(*N*-isopropyl acrylamide) Across the Volume Phase Transition Compared to its Monomer. *Sci. Rep.* **2017**, *7*, 17012.

(78) Rubio Retama, J.; Frick, B.; Seydel, T.; Stamm, M.; Fernandez Barbero, A.; López Cabarcos, E. Polymer Chain Dynamics of Core-Shell Thermosensitive Microgels. *Macromolecules* **2008**, *41*, 4739−4745.

(79) Grinberg, V. Y.; Senin, A. A.; Grinberg, N. V.; Burova, T. V.; Dubovik, A. S.; Potekhin, S. A.; Erukhimovich, I. Y. High Pressure Effects under Phase Separation of Aqueous Solutions of Poly(*N*-isopropylacrylamide): A HS-DSC Study. *Polymer* **2015**, *64*, 14−18.

(80) Metzler, R.; Jeon, J.-H.; Cherstvy, A. G.; Barkai, E. Anomalous Diffusion Models and their Properties: Non-Stationarity, Non-Ergodicity, and Ageing at the Centenary of Single Particle Tracking. *Phys. Chem. Chem. Phys.* **2014**, *16*, 24128−24164.

(81) Laage, D.; Stirnemann, G.; Hynes, J. T. Why Water Reorientation Slows Without Iceberg Formation around Hydrophobic Solutes. *J. Phys. Chem. B* **2009**, *113*, 2428−2435.

(82) Sterpone, F.; Stirnemann, G.; Hynes, J. T.; Laage, D. Water Hydrogen-Bond Dynamics around Amino Acids: The Key Role of Hydrophilic Hydrogen-Bond Acceptor Groups. *J. Phys. Chem. B* **2010**, *114*, 2083−2089.

(83) Li, H.; Yamada, H.; Akasaka, K. Effect of Pressure on Individual Hydrogen Bonds in Proteins. Basic Pancreatic Trypsin Inhibitor. *Biochemistry* **1998**, *37*, 1167−1173.

(84) Dougherty, R. C. Temperature and Pressure Dependence of Hydrogen Bond Strength: A Pertubation Molecular Orbital Approach. *J. Chem. Phys.* **1998**, *109*, 7372−7378.

(85) Ramon, O.; Kesselman, E.; Berkovici, R.; Cohen, Y.; Paz, Y. Attenuated Total Reflectance/Fourier Transform Infrared Studies on the Phase-Separation Process of Aqueous Solutions of Poly(*N*-isopropylacrylamide). *J. Polym. Sci., Part B: Polym. Phys.* **2001**, *39*, 1665−1677.

(86) Ghosh, T.; García, A. E.; Garde, S. Enthalpy and Entropy Contributions to the Pressure Dependence of Hydrophobic Interactions. *J. Chem. Phys.* **2002**, *116*, 2480−2486.

(87) Smuda, C.; Gemmecker, G.; Unruh, T. Quasielastic and Inelastic Neutron Scattering Study of Methyl Group Rotation in Solid and Liquid Pentafluoroanisole and Pentafluorotoluene. *J. Chem. Phys.* **2008**, *128*, 194502.

(88) Doster, W.; Settles, M. Protein-Water Displacement Distributions. *Biochim. Biophys. Acta, Proteins Proteomics* **2005**, *1749*, 173−186.